Structure of Amorphous Starch. 1. An Atomistic Model and X-ray Scattering Study

U. Trommsdorff* and I. Tomka

Institute for Polymers, Swiss Federal Institute of Technology Zurich, ETH-Zentrum, CH-8092 Zurich, Switzerland

Received December 12, 1994; Revised Manuscript Received May 23, 1995[⊗]

ABSTRACT: A detailed atomistic model for dry amorphous starch was simulated using an established method that proved useful for several technical polymers. Two currently available force fields were tested for their ability to simulate carbohydrates. The model structures showed that the interactions between the starch molecules are dominated by the interactions of the polar hydroxyl groups. They built hydrogen bonds, both *inter-* and *intra*molecular, and occurred in a wide variety of geometries, including three-center bonds. The model corroborated the high cohesive energy density of starch and showed that the latter correlates with the density of *inter*molecular hydrogen bonds. The differential radial distribution function for amorphous starch was evaluated from X-ray scattering measurements as well as from the model structures, and the agreement was good up to distances of 6 Å. It was shown that this function is dominated by *intra*molecular correlations, which overlay the *inter*molecular ones occurring mainly at hydrogen-bonding distances.

Introduction

Substances from natural resources are gaining increasing importance as components for working materials because they are biodegradable and renewable. Starch is a natural polymer that is available worldwide at low cost. It can be extracted from various plants, such as maize, rice, potatoes, and wheat, and has long been used for practical purposes.[1] Starch is made of linear (amylose) and branched (amylopectin) α-linked chains of D-anhydroglucose. It can be transformed into a thermoplastically processable material through a thermomechanical treatment and the use of a suitable plasticizer.[2–5] This thermoplastic starch has an amorphous structure,[6] whereas the native material occurs in partially crystalline form. The crystal structures of native starch vary with the plant they originate from and have been investigated extensively.[7] It is generally accepted that they are made of double helices which are packed differently.[8] The amylose molecule and the branching point regions of the amylopectin molecule form the amorphous part of the starch granule, which amounts to 55–85% of the total.[7,9] The amylose is found in the central part of the granule and between the crystal lamellae.[7,9] Model calculations of the branching point regions have shown that they do not induce extensive defects into the double-helical structure but instead serve to initiate the crystalline arrangement.[10,11] In amorphous amylose and ethanol-precipitated gelatinized starch, a substantial amount of the molecules adopt single-helical *local* conformations, as has been suggested by results of solid-state NMR measurements.[12,13] However, little is known about the interactions between the molecules in the amorphous bulk material, and the solution conformation of the amylose molecule is still a matter of debate.[14–17]

Dry starch is extremely hydrophilic and under normal atmospheric conditions starch, like other biological materials, always contains water. In fact, this hydrophilic behavior is the most severe argument against its use as a working material and has led to the search of alternative plasticizers.[18] In this study we investigate the amorphous structure of dry starch on a molecular level using X-ray diffraction and molecular modeling. In the succeeding contribution[19] the investigation was extended to amorphous structures containing water.

The first detailed atomistic simulation of an amorphous polymeric system at densities corresponding to the glassy state was performed by Theodorou and Suter[20] for polypropylene. Since then, their method has been successfully used to simulate other polymers such as PC,[21] PVC,[22] and PS.[23] Applications of these structures include studies on the diffusion of small molecules,[24–26] the modeling of chain dynamics in PC[27] and of the dynamics of the local motion of the phenyl groups in PS,[23] and the study of mechanical properties.[28–31] A detailed review on the modeling of glassy polymers can be found in Gentile and Suter.[32]

This study presents a model for the dry amorphous starch structure using the basic assumptions of the Theodorou–Suter method. Since the system was simulated through explicitly treating the interactions between all atoms, the choice of the interaction parameters and the mathematical formulation of the various interactions, i.e., the force field, was of major importance. The functional forms and also the way of parametrization is different in the various proposed force fields, so that parameters usually cannot be interchanged. Two force fields were tested for their ability to simulate structures which contain glucopyranose units, and the results are presented below.

The structural information that can be gained from X-ray scattering experiments on isotropic amorphous materials is contained in the differential radial distribution function[33] $4\pi r^2\Delta\varrho^x(r)$. It describes the radially averaged difference $\Delta\varrho(r)$ between the local and the mean density of atoms at a distance r around an arbitrary atom. At high distances, this function tends to zero, i.e., the local density corresponds to the mean atomic density in the system. At distances of a few atomic radii, however, the local density is determined by the *inter-* and *intra*molecular distance relations of the neighboring scatterers. The model calculations allowed an interpretation of the local structural relations which appear in an averaged way in the differential radial distribution function. (Note that the index "x" in $4\pi r^2\Delta\varrho^x(r)$ refers to X-ray scattering.)

[⊗] Abstract published in *Advance ACS Abstracts,* August 1, 1995.

0024-9297/95/2228-6128$09.00/0

Selection of the Force Field

The geometry and the conformations of maltose, the dimer of D-anhydroglucopyranose, as well as the double helix of the crystal structure of starch were simulated with two different force fields: (1) the PCFF91 force field of BIOSYM,[34,35] which contains no special parameters for carbohydrates, and (2) the Amber force field.[36,37] All energy minimization and molecular dynamics calculations were performed with the Discover molecular modeling software (version 2.9) of BIOSYM Technologies.[38]

The PCFF91 force field uses ab-initio potential energy surfaces of small molecules and a rigorous methodology to derive the parameters that describe the potential energy of a system of atoms.[39-41] This force field is designed to account for properties of very diverse systems, i.e., isolated small molecules, condensed systems, and macromolecules. It uses anharmonic functional forms to describe bond stretching, angle bending, and torsion. Cross terms, linking angle, and bond and torsion deformation have also been found to be important for an accurate description of the potential energy of a molecule. Furthermore, the PCFF91 force field contains a term for the Coulombic interaction of the partial atomic charges and one for the van der Waals interaction.

The Amber force field, on the other hand, has a very simple form, containing quadratic terms for the bond stretching and angle bending, a simple torsion potential, and no cross terms. Two additional conditions are (1) that the van der Waals and Coulombic interactions between atoms that are separated by three bonds are reduced to 50% and (2) that a distance-dependent dielectric constant $\epsilon(r) = \epsilon r$ is usually used. The hydrogen bonds are described by Coulombic and van der Waals interaction. Parameters for the Amber force field suitable for carbohydrates have been proposed by Homans.[42] They have been used in the following calculations, with the modification that the data of the standard glucopyranose geometry[43,44] have been inserted for the reference values of bonds and angles.

The geometry of the maltose molecule (Figure 1b), the α-linked dimer of D-anhydroglucopyranose (Figure 1a), was simulated[45] and the most consistent results with the X-ray diffraction data of glucopyranose were achieved with the Amber force field using a distance-dependent dielectric constant ($\epsilon = 4r/$Å), i.e., almost complete shielding of the partial charges. Stronger coulombic forces ($\epsilon = r/$Å) distorted the ring. With the PCFF91 force field, good agreement of the bond and torsion angles with the standard geometry was obtained, and the ring conformation proved to be more stable toward changes in the strength of the Coulombic interaction. However, the bond lengths in the glucopyranose ring came out longer by ca. 2% than in the standard structures. Furthermore, the anomeric effect[46] of a shortened $C(1)-O_g$ bond length was not properly accounted for, since the PCFF91 force field does not contain parameters specific to the anomeric linkage. The bond length of $C(1)-O_g$ was simulated too long by 2%.

The potential energy surface for the conformation angles ϕ and ψ (for a definition, see Figure 1b) in α-maltose was simulated with both force fields,[45] and they showed a shape comparable to the ones reported in the literature.[16,47,48] Figure 2 shows the potential energy surface calculated with the PCFF91 force field. Two main regions can be distinguished: region I is centered at ϕ and ψ values around 0°, region II is characterized by ψ-angles around 180°. Conformation

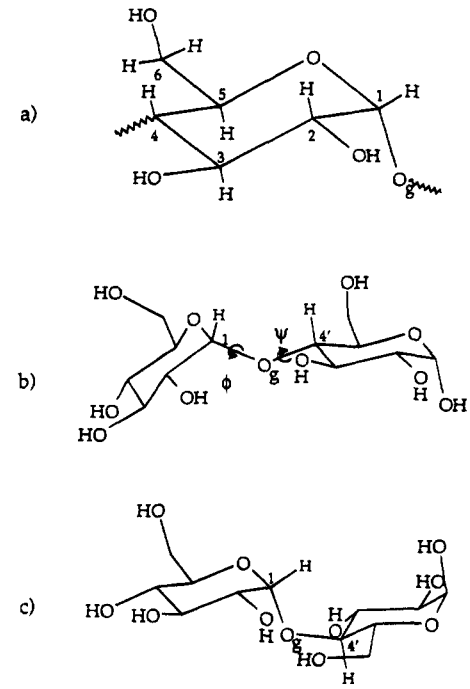

Figure 1. (a) Representation of the α-D-anhydroglucopyranose unit. (b) Maltose molecule with conformation angles ϕ and $\psi < 0$ and (c) with conformation angles ϕ and $\psi > 0$. The conformation angle ϕ is measured from the $H(1)-C(1)-O_g-C(4)'$ torsion angle and ψ from $C(1)-O_g-C(4)'-H(4)'$. The subscript "g" is used for the glycosidic oxygen atom linking the two subunits of the maltose molecule.

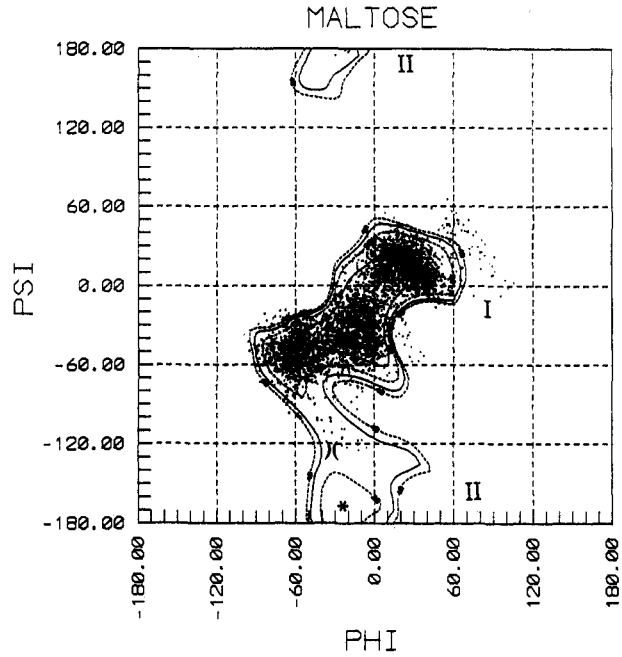

Figure 2. Potential energy surface of maltose (rigid geometry) for the conformation angles ϕ and ψ. Contours are shown in 10 kcal/mol intervals above the minimum. I and II denote the two main conformation angle regions. Dots show the conformation angle pairs ϕ and ψ visited during a MD simulation (see text for details).

angles from region I have been found in crystal structures of maltose and similar small molecules and also in the different helices of starch, or amylose.[47,49,50] Conformations from region II (Figure 1c) have (to the authors' knowledge) only been confirmed experimentally to occur in maltose solutions.[51] The dots in Figure 2 show the conformation angle pairs that were visited during a molecular dynamics simulation (100 ps, 300 K, sampling every femtosecond) of maltose. The mol-

ecule was found in the whole conformation space enclosed by the contour line of 40 kcal/mol relative to the minimum that had been calculated for the rigid geometry. Furthermore, three subregions of conformations that were not detected in the rigid-geometry map can be distinguished. These are related to the three stable conformers described by Pérez and Vergelati[16] and have been found also in the flexible-geometry conformation maps of Tran et al.[48] and Ha et al.[52] as well as in the MD simulations of Brady and Schmidt.[53] No transitions between regions I and II of the conformation map were observed in simulations that have been started from a conformation of region I (also observed by Ha et al.[52]). This is consistent with the higher energy barrier for the I → II transition which was calculated for the rigid-geometry conformation map (Figure 2) and which was also found in flexible-geometry conformation maps.[48,54]

A simulation of a section of the double helix of starch with the PCFF91 force field showed a fiber repeat distance that is within 1% and conformation angles at the glycosidic linkage that are within 5% of the values[45] reported from X-ray data.[55] Furthermore, the hydrogen bond structure agreed with these data. However, since the structure was simulated in vacuum, instead of the dimeric and trimeric repeat units, which result from the symmetry relations in the A- and B-crystal structures,[55,56] a monomeric repeat unit was found. The agreement was less satisfactory with the Amber force field, and an additional *intra*molecular hydrogen bond was found.

The results obtained with the PCFF91 force field for the geometry of the repeat unit of starch, the potential energy surface of maltose, and the double-helix structure show that this force field is suitable for the simulation of starch structures. In contrast to simulations with the Amber force field, the pyranose ring was stable toward changes in the strength of the Coulombic interaction, and the hydrogen bond structure of the simulated double helix corresponded to experimental data. The stability of the ring is important in the simulations of the dense system because in the initial stages of the simulation, unfavorable geometrical arrangements of the molecule may occur, which should not be "equilibrated" through the deformation of the sugar ring. However, deviations from the crystallographic mean data for bond lengths were obtained with the PCFF91 force field, which are of the order of 2%, and the anomeric effect was not accounted for.

Model for Amorphous Starch

Methods. The glassy starch structures were modeled in cubic cells with periodic continuation conditions[57] obeying the minimum image convention.[58] The following two assumptions of the Theodorou–Suter method[20] have been used: (1) the glass was seen as a state of frozen-in liquid disorder and the temperature entered only through the specification of the density, i.e., the model was static; (2) the polymer was represented as an ensemble of microstructures, each of which is in a local minimum of the potential energy. A further assumption was that the amorphous structure of thermoplastic starch, which consists of linear and branched molecules, can be modeled by linear (amylose) chains only.

Different strategies to generate microstructures of glassy polymers can be envisaged that consist of a suitable combination of the generation of a starting chain conformation and the relaxation of the system to reach minimal potential energy. The high density of glassy polymeric systems and the extremely long relaxation times of the polymers under these conditions have the effect that (with the available computer power) the conformation of the simulated chain is strongly influenced by the starting structure (initial guess structure). Here for the starting structure an *energy-biased chain "polymerization" method* was performed, and the relaxation was achieved through a combination of molecular dynamics and energy minimization.

The simulation box contained *one* single chain of amylose and its size was defined by the choice of the density of the initial guess structure and the length of the chain. The chain was allowed to grow out of the box and through the periodic continuation conditions, it was assured that an image of the chain enters the simulation box according to the cubic symmetry. In this stage of the simulation the rigid standard geometry was used for the repeat units and the system was not relaxed between steps. The first repeat unit was filled into the box by choosing place and orientation at random. The energy-biased "polymerization" method then lets the chain grow by repeating the following procedure for every repeat unit: (1) the potential energies of interaction between the repeat units to be added and those already "polymerized" are calculated for a number of conformations defined by the pair of conformation angles ϕ and ψ at the new linkage (ϕ between −100 and 80° and ψ covering the entire angle space every 5°; compare Figure 1b); (2) the Boltzmann weights of these conformations are evaluated and "lined up" on a ruler of length 1; (3) one of the conformation angle pairs is chosen with a random number between 0 and 1 and the repeat unit is added correspondingly.

In contrast to methods that select conformations of the chain from a dimeric conformation map,[14,16,59] this method includes interactions beyond the two units to be linked. It ensures that conformations that lead to low energies of the *whole system* get a better chance to be selected and therefore leads to simulation boxes that are evenly filled.[20]

Several initial guess structures were prepared at different starting densities with the procedure described. The degree of polymerization of the amylose chain was 80 in all cases. The initial guess structures then had to be compressed to reach the density of amorphous starch (1.5 g/cm^3 [60,61]). For this, they were—after a short energy minimization to relax possible "hot spots" (places with high potential energies)—subjected to molecular dynamics at constant pressure (*NPT*). The temperature was kept constant at 300 K using velocity rescaling during the initialization period and temperature bath coupling[62] during the data collection period (*characteristic relaxation time: 100 fs*), and the pressure was maintained by coupling to a pressure bath[62] (*compressibility* 5×10^{-5} *bar*$^{-1}$ *and relaxation time constant 100 fs*). The integration was performed using the Verlet algorithm[63] with a time step of 1 fs. With the *NPT* molecular dynamics at a pressure that just corrects for the cutoff used in the simulations, the structures attained a density of 1.3 g/cm^3. To reach the experimental density of amorphous starch, higher pressures had to be applied. After the compression stage of the simulation, the structures were allowed to relax during constant volume (*NVT*) molecular dynamics, which was continued until a reasonably constant total energy was reached. The total molecular dynamics simulation time was approximately 20 ps.

Finally, the structures were subjected to an energy minimization to reach a gradient in the potential energy

Table 1. Results for the Model Structures Started at Different Densities[a]

	density of the initial guess (g/cm³)		
	0.001	1.00	1.50
potential energy of the minimized structures			
E_{pot}	−481 (±101)	−504 (±50)	−441 (±23)
E_{int}	−1772 (±24)	−1795 (±18)	−1717 (±24)
E_{vdW}	−394 (±24)	−411 (±34)	−434 (±9)
E_C	1686 (±18)	1701 (±35)	1728 (±21)
no. of glycosidic linkage conformations in I	71 (90%)	61 (77%)	54 (68%)
$r_{end\text{-}to\text{-}end}$ (Å)	147 > 32	80 > 69	99 > 98
initial guess > end structure			
total computation time per structure (CPU hours on a Cray YMP)	10.6	6.8	6.2
pressure (bar)	16453 (±2793)	16121 (±1583)	13854 (±856)
total energy after MD	2648 (±107)	2619 (±48)	2677 (±21)

[a] The results are averages of the three microstructures; the rms deviation is given with parentheses. All energies are given in kcal/(mol of microstructures).

of less than 0.01 kcal/(mol Å). The energy minimization algorithms used were the steepest descent method for the first ten steps and the conjugate gradient method for the following steps. (Note that the applied strategy to generate microstructures for glassy starch is purely empirical and does not claim to have any physical meaning nor to be the only possible one.)

During the compression and relaxation stages of the simulation, the potential energy was calculated using a cutoff of 10 Å (smoothed by a quintic spline function between 9.5 and 10 Å). Furthermore, neutral charge groups were used for the summing-up of the non-bond energy terms to ensure the electrical neutrality of the system within the cutoff. The bond lengths, bond angles, and torsion angles of the molecules were not constrained in any way and the full non-bond energy function was applied. The Discover modeling software (version 2.9) of BIOSYM Technologies[38] was used for the energy minimizations and the molecular dynamics. Most calculations were performed on a Cray YMP at the ETH Zurich.

Influence of the Starting Density. The high density and the large number of degrees of freedom in the glassy structures would require annealing times that cannot be accomplished with current computers to get rid of the influence of the starting structure. To assess the extent of this influence, a set of three microstructures each was started at three different densities corresponding to a fictitious gaseous state (0.001 g/cm³), the partial density of the starch component in amorphous starch with 18% of water (1.0 g/cm³), and the experimental density of amorphous starch (1.5 g/cm³). Table 1 compares the mean values of the energies, the conformation distribution, and the end-to-end distances of the chains in these microstructures for amorphous starch simulated with the above-described method.

It was found that the distribution of the conformation angles at the glycosidic linkage and the end-to-end distance, i.e., the conformation of the chain, could be varied by the choice of the density for the initial guess structure. Using a large box, i.e., a low density, the chain grew into an extended helical conformation. In smaller boxes, i.e., at higher densities, the long-range interactions became more important and also $\phi-\psi$ conformation angles pairs that lead to higher *intra*molecular energies were selected. The helical character of the growing chain was then less pronounced. The generation of an initial guess structure at the lowest density resulted in a higher number of region I conformations and, although the chain got coiled during the compression, most of the conformations of the final

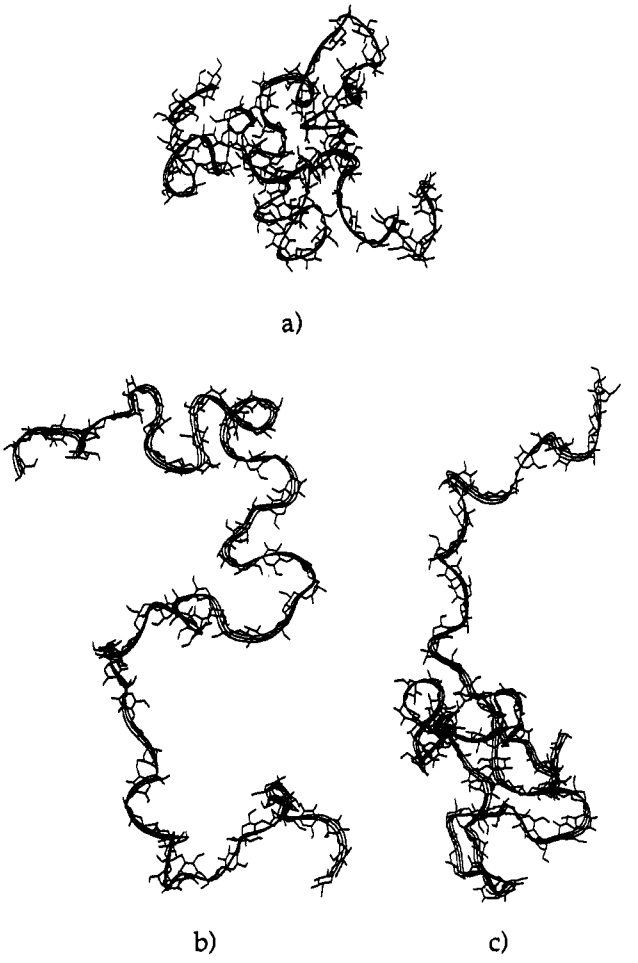

Figure 3. Selected chains of the three types of model structures, which had been started at a density of (a) 0.001, (b) 1.0, and (c) 1.5 g/cm³. Hydrogen atoms are not displayed and a ribbon is drawn along the backbone for clarity.

structure (Figure 3a) were from region I of the dimer conformation map. The coiling is also seen in the strong decrease of the end-to-end distance ($r_{end\text{-}to\text{-}end}$ in Table 1). (Note that these structures require 30% more computing time than the others.) Starting structures calculated at the experimental density of dry starch (1.5 g/cm³) did not change their end-to-end distances and conformation distributions much during the relaxation, and they contain a substantial amount of region II conformations (Figure 3c). An intermediate situation was reached in the structures started at the intermediate density (Figure 3b). The conformation angle pairs of the three types of structures were broadly distributed in the low-energy regions given by the dimer conformation map. The existence of conformations from region

II (high ψ-angles) in *polymeric* D-anhydroglucose systems has not yet been assessed experimentally.

Note that the end-to-end distance of an amylose chain of 80 repeat units of 4.5 Å length in a Θ-solvent is 85 Å, taking C_∞ from light scattering measurements.[17] Using the assumption that the polymer remains in its unperturbed conformation in the amorphous state,[64] the end-to-end distances of the structures started at the higher densities have been selected to lie within 20% of this value.

The total energy of the microstructures at 300 K and the potential energy of the minimized structures are very similar in all the modeled systems in spite of the different methods of construction. The upper part of Table 1 displays the internal energy (E_{int}), the van der Waals (E_{vdW}), and the coulombic energy term (E_C), which together form the total potential energy (E_{pot}). The internal energy contains contributions from the bond, angle, and torsion deformations. The negative internal energy term and the positive Coulombic energy term are artifacts of the force field and do not imply that the *intermolecular* Coulombic energy of the structures was negative (see below). The systems started at lower densities showed a higher fluctuation of the potential energy as well as of the pressure and the total energy. This might be an effect of the stronger coiling of the amylose chain during the compression step and an extension of the length of the simulation could possibly reduce the deviation.

The last three rows of Table 1 show the pressure and the total energy from the *NVT*-dynamics simulation prior to the minimization. In all the structures the pressure that was used to adjust the density of the simulated system was very high. This is most probably an effect of the force field and not of the method of constructing the model. To show this, constant-volume molecular dynamics was continued for 7.5 ps for the microstructures, started at a density of 1.0 g/cm^3 using the Amber force field. The pressure was then much lower, namely, 3122 bar (with a fluctuation of 1843 bar). These structures were also energy-minimized and the resulting hydrogen-bonding density was approximately the same as with the PCFF91 force field. The cohesive energy density came out ca. 10% lower. An optimization of the force field to match carbohydrates could solve these shortcomings.

Differential Radial Distribution Function $4\pi r^2\Delta\varrho^x(r)$ from Measurement and Model

X-ray Scattering Experiments. Amorphous thermoplastic starch was produced from native potato starch (Blattmann & Co., Wädenswil CH), which showed a high-temperature transition[5] at 181 °C (at 18% water) and an intrinsic viscosity of 314 mL/g. The starch was processed with 27% of water in a BUSS extruder (temperature 101−102 °C; introduced mechanical work, 0.21−0.24 kwh/kg) and granulated. The intrinsic viscosity was 115.6 mL/g after the melting process.

For the first sample the granulate was ground in a mortar to a fine powder. For the second sample the granulate (18% water) was melted and formed into a platelet with 1 mm thickness in a press at 130 °C. Both samples were dried until their weight was constant (approximately 2 weeks for the powder and 2 months for the plate) in a vacuum oven at 80 °C over P_2O_5. The residual water content was less than 0.01% (powder) and 0.5% (plate). The X-ray scattering experiments were performed on a SCINTAG PADX θ/θ diffractometer using a solid-state detector for Cu Kα radiation. The powdered sample was measured at room temperature and the platelet at 25 K in a low-temperature attachment with a closed-cycle helium cryostat. The angular range was 2−140° 2θ, the step size was 0.05°, and the recording time per step was 30 s.

Furthermore, the measurements were repeated at the same conditions but with an empty cell to record additional scattering from air or from the sample holder.

Outline of the Theory and Data Treatment. The theoretical ground to relate the intensity of X-ray scattering of a noncrystalline structure to the positions of the atoms was laid by Debye,[65] and extensive descriptions of all the derivations can be found in Klug[33] and Warren.[66] The coherent intensity $I(q)$, expressed in units of the scattering amplitude of a single electron (electron or Thompson units, eu) scattered by a structural unit of the observed system, can be written as

$$I(q) = \sum_\alpha N_\alpha f_\alpha^2(q) + \sum_\alpha \sum_\beta f_\alpha(q) f_\beta(q) \int_0^\infty 4\pi r^2 \Delta\varrho_{\alpha\beta}(r) \frac{\sin(qr)}{qr} \mathrm{d}r \quad (1)$$

where $q = 4\pi \sin(\theta)/\lambda$ is the length of scattering vector at half the scattering angle 2θ and λ is the wavelength of the X-rays; $f_\alpha(q)$ and $f_\beta(q)$ are the atomic scattering factors of the α- and β-atoms. N_α is the number of α-atoms per structural unit, and the summations have to be taken over one structural unit of the system. $4\pi r^2\Delta\varrho_{\alpha\beta}$ is the differential radial distribution function, which describes the radially averaged difference $\Delta\varrho(r)$ between the local and the mean density of β-atoms at the distance r around an α-atom and vice versa. Since the scattering power of the different atoms can only be included in an averaged way (using a mean scattering factor $f_e(q) = \sum N_\alpha f_\alpha(q)/\sum Z_\alpha N_\alpha$, with Z_α the number of electrons in the α-atom), the superscript "x" is used to indicate the differential radial distribution function obtained from coherently scattered X-ray intensity by an inverse Fourier transform:

$$4\pi r^2\Delta\varrho^x(r) = 4\pi r^2 \mathcal{F}^{-1}\left\{\frac{I(q) - \sum f_\alpha(q)^2}{f_e^2(q)}\right\} \quad (2)$$

The coherently scattered intensity $I(q)$ has to be provided in absolute units. Therefore, the measured intensity $I_{meas}(q)$ had to be corrected for the "empty cell" scattering $I_{add}(q)$, polarization $P(q)$, absorption $A(q)$, and incoherent scattering $I_{inc}(q)$ and to be scaled (K) to absolute units (e.g., Klug[33] and Alexander[67]). The correction for multiple scattering has been omitted, because it is of the order of some percent of the intensity only.[68] The measured intensity was therefore made up in the following way:

$$I_{meas}(q) = I_{add}(q) + KP(q)A(q)[I(q) + I_{inc}(q)] \quad (3)$$

The "empty cell" scattering from air (low angles) and from the sample holder (higher angles) was subtracted from the intensity of the sample (taking into consideration the absorption by the sample). The correction for absorption and polarization was done following standard procedures.[33] The absorption coefficient of starch was calculated from the mass absorption coefficients tabulated in the *International Tables of X-ray Crystallography*.[69]

The analytical approximation of Smith et al.[70] was used for the incoherent scattering with a correction[71]

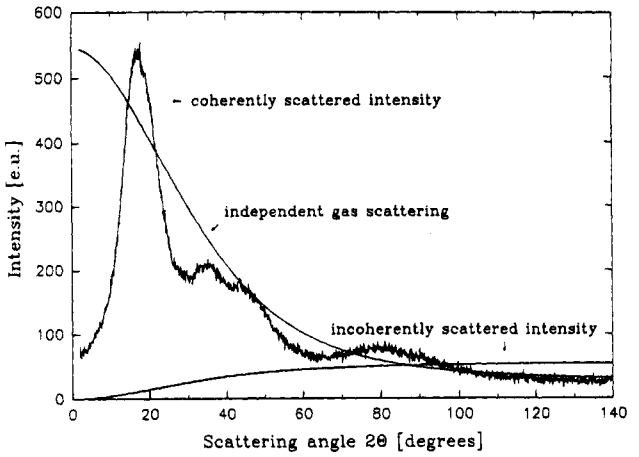

Figure 4. Coherent intensity, independent gas scattering (sum of atomic scattering factors of the repeat unit), and incoherent scattering of dry starch (platelet) in electron units (eu).

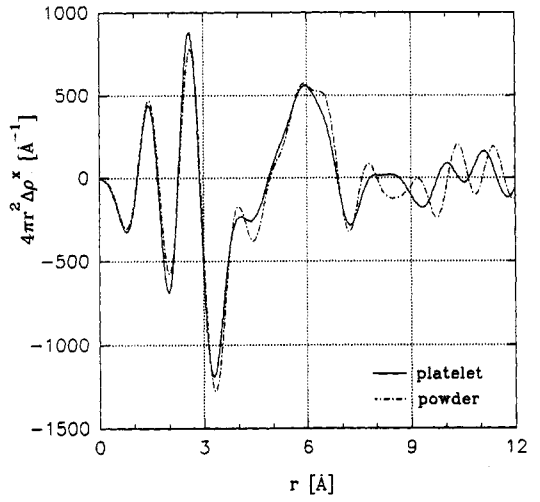

Figure 5. Differential radial distribution function of dry starch calculated from experimental data measured for a powder and a platelet sample.

to account for the fact that the electrons are not free (Breit–Dirac factor). The method of Krogh-Moe[72] was used for the scaling of the intensity to absolute units, and the atomic scattering factors $f_\alpha(q)$ have been taken from Yanez and Steward.[73] To avoid spurious peaks[33] caused by the limited scattering angle region accessible to the experiment, the reduced intensity was multiplied with a suitable damping function.[74]

Figure 4 shows the coherent intensity, independent gas scattering, and the incoherent scattering of the measured starch sample. Since these measurements were performed in symmetrical reflection, the interpretation of the high-distance region of the calculated differential radial distribution function is limited by the accuracy of the measurement at low scattering angles due to the quality of the surface of the sample.[33] To get an idea of where this limit had to be set, the scattering intensity of dry starch was measured of a powdered sample and of a platelet. Figure 5 shows the differential radial distribution function of the two different samples. The results suggest that the range of validity of the differential radial distribution function, as calculated from the performed scattering experiments, is limited to distances below 8 Å.

Evaluation of $4\pi r^2\Delta\varrho^x(r)$ from Model Data. The differential radial distribution function can be calculated from model data by combining eqs 1 and 2 and using

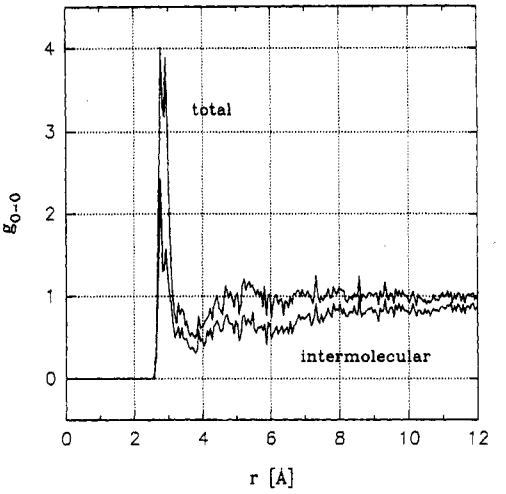

Figure 6. Total and *inter*molecular radial pair distance distribution function g_{O-O} of the hydroxyl-oxygen atom pairs.

the pair distribution functions $g_{\alpha\beta}(r)$ of the atom pairs $\alpha\beta$ calculated from the model structures. The latter are related to the differential distribution functions $\Delta\varrho_{\alpha\beta}(r)$ in the following way:

$$\Delta\varrho_{\alpha\beta}(r) = \frac{N_\alpha N_\beta}{V}(g_{\alpha\beta}(r) - 1) \tag{4}$$

where $N_\alpha N_\beta/V$ is the density of $\alpha\beta$-pairs in the system. To compensate for the fact that the model structures are static, i.e., to account for interatomic distance fluctuations, the pair distribution functions have been convoluted with the Debye–Waller temperature factor $\exp(-\sigma^2q^2)$, where σ^2 is a measure of the mean square displacement of the atoms from their equilibrium position due to thermal vibration. The function $4\pi r^2\Delta\varrho^x(r)$ was calculated in the following way:

$$4\pi r^2\Delta\varrho^x(r) = 4\pi r^2\frac{P}{V_c}\sum_\alpha\sum_\beta N_\alpha N_\beta W_{\alpha\beta}(r) \otimes (g_{\alpha\beta}(r) - 1)$$

$$W_{\alpha\beta}(r) = \mathcal{F}^{-1}\left\{\frac{f_\alpha(q)f_\beta(q)}{f_e^2(q)}\exp(-\sigma^2q^2)\right\} \tag{5}$$

with V_c being the size of the model cube, N_α and N_β the number of α- β-atoms, respectively, in a structural unit, and P the number of structural units in the model cube.

The convolution

$$A(r) \otimes B(r) = \int_{-\infty}^{\infty} A(R)B(|r-R|)\,dR$$

was performed after extending both functions to negative r-values by symmetrical reflection at $r = 0$.

Results and Discussion

Hydrogen Bonds. The high number of polar hydroxyl groups in the starch molecule suggests a rich hydrogen-bonding structure in these systems, which could be investigated in detail in the model structures. Figure 6 shows the total and the *inter*molecular radial distribution function, g_{O-O}, of the hydroxyl oxygen pairs. A pronounced double peak is seen slightly below 3 Å, ranging from 2.6 to 3.1 Å. This indicates that, unlike in proteins, there exists a variation in the lengths of hydrogen bonds that is comparable to the range of distances found in crystal structures of small carbohydrates.[46,75] Because there is no unambiguous definition

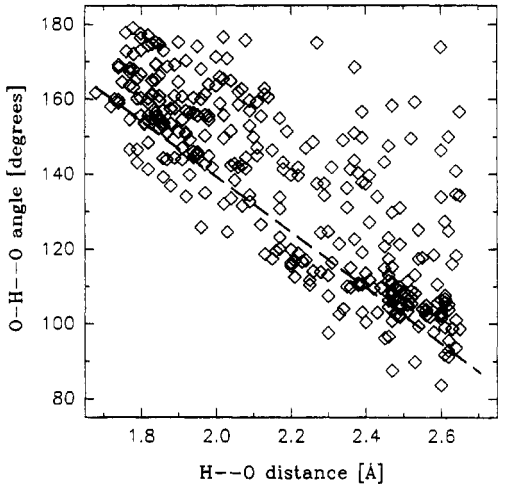

Figure 7. Hydrogen bond angles (O−H···O) in degrees plotted against hydrogen bond distances (O···H) in angstroms. Dashed line adapted from Savage and Finney.[76]

of a hydrogen bond in terms of the interaction energy of the involved atoms,[53] a geometrical description had to be chosen. From the two general rules that have been formulated for hydrogen bonds in crystal structures of carbohydrate structures,[46] which are (1) to maximize the hydrogen bond interactions by including all hydroxyls and as many ring and glycosidic oxygens as possible, using both two- and three-center bonds, and (2) to maximize cooperativity by forming as many finite and infinite chains of hydrogen bonds as possible, the following practical rules have been derived:

(1) All hydrogens belonging to hydroxyl groups and all oxygen atoms in the starch molecules were considered.

(2) A pair of a hydrogen and an oxygen atom was considered to be hydrogen bonded if their distance is smaller than 2.25 Å. Pairs with higher distances (2.25–2.65 Å) were also considered hydrogen bonded if they form part of a three-center bond.

"Three hydrogen bonds per repeat unit" (or per molecule) signifies that every repeat unit (or molecule) was connected by three hydrogen bonds to some other repeat units (or molecules).

An inspection of the model structures revealed the wide variety of hydrogen bond geometries. Figure 7 shows the hydrogen bond angle plotted against the distance between the oxygens. There exists a lower boundary beneath which angle/distance combinations are not found because of restrictions due to repulsive interactions between the participant atoms. This boundary is comparable to the one found for hydrogen bonds in water and in crystalline hydrates.[76]

On the average, every repeat unit made 7.8 hydrogen bonds in the model structure. The total number of hydrogen bonds was not very different in the three model types and lay within ±3% of this value. The number of *inter*molecular hydrogen bonds, however, was lower in the model structures started at a low density. There the molecule was coiled, which led to an increased number of *intra*molecular hydrogen bonds (discussed below).

The hydrogen-bonding situation of one selected microstructure was further investigated in detail. It contained 7.8 hydrogen bonds per repeat unit, of which 56% were *inter*molecular bonds. Table 2 shows the number of hydrogen bonds associated with the 5 oxygen atoms of each repeat unit. As one would anticipate, most (6.9 per repeat unit or 88%) of the hydrogen bonds

Table 2. Distribution of Total, *Inter*molecular, and *Intra*molecular Hydrogen Bonds on the Different Hydrogen-Bonding Groups of a Repeat Unit for One Selected Microstructure[a] and Fraction of Hydroxyl Groups, Which are Donor *and* Acceptor

group	total	*inter*molecular	*intra*molecular	donor and acceptor
OH(2)	2.58	1.37 (53%)	1.21 (47%)	75%
OH(3)	2.36	1.21 (51%)	1.15 (49%)	59%
OH(6)	1.96	1.43 (73%)	0.53 (27%)	62.5%
O(5)	0.44	0.28 (63%)	0.16 (37%)	
$O_{glyc.}$	0.46	0.11 (24%)	0.35 (76%)	
total	7.80	4.40 (56%)	3.40 (44%)	65%[b]

[a] Units are number of hydrogen bonds per group. In parentheses: fraction with respect to the total number of hydrogen bonds per selected group. [b] Fraction of all hydroxyl group hydrogen bonds.

contained one of the hydroxyl groups. The hydroxyl group of the C(6) carbon atom was the most flexible, with the maximum number of *inter*molecular hydrogen bonds. The OH(2) group was the one that was most often involved in *intra*molecular hydrogen bonds. More than half of the hydroxyl groups were donors as well as acceptors. This is less than in crystal structures of similar small molecules, where each hydroxyl group is always both donor and acceptor.[75]

Due to the deficit of hydrogen bond donors, three-center hydrogen bonds occurred. In crystal structures of small saccharides the fraction of three-center bonds approximately corresponds to the surplus of acceptor over donor atoms.[46] The model structures of amorphous starch contained 67% more oxygen than hydroxyl hydrogen atoms and approximately 40% of the donor atoms were bonded to two acceptor atoms. The length of the two branches of the bifurcated donor bond was slightly different, which explains the double peak observed in the pair distribution function of the hydroxyl oxygens (Figure 6).

The Cohesive Energy Density. The dense network of hydrogen bonds described above indicates strong interactions between the molecules. Indeed the cohesion energy density of starch, similar to the one of cellulose, is 3−4 times higher than for apolar polymers such as polypropylene. The cohesive or the *inter*molecular energy of the simulated structures was calculated by evaluating the difference of the total potential energy of the chain in the cube to the total potential energy of the naked chain in vacuum.[20] The former was calculated with a cutoff equal to half of the box size (12.15 Å, without the spline function used during molecular modeling calculations to smooth the cutoff), and a correction term was estimated separately to take into account the non-bond energy function for the longer distances. The correction term for the van der Waals energy was calculated analytically by assuming that the pair distribution functions of the different atom pairs were constant for distances greater than the cutoff. It equaled −76 kcal/(mol of microstructure) and hence contributed ca. 5% to the total *inter*molecular energy. For the correction of the Coulombic energy, two methods were tested: (1) the reaction field method (e.g., Allen and Tildesley[77]), which overestimates the continuum nature of the system, and (2) a method analogous to the Ewald summation (e.g., Allen and Tildesley[77]), using explicit images of the chain to extend the cutoff, i.e., overestimating the periodicity of the system. In both cases the Coulombic correction term was smaller than 10 kcal/(mol of microstructures), which is less than 1% of the total *inter*molecular energy, and was omitted.

Table 3. Cohesive Energy Density E_{coh}/V (Uncorrected), van der Waals E_{vdW} and Coulombic E_C Parts of the Cohesive Energy, Correction Term $\Delta E_{el}/V$ for the Cohesive Energy Density, Solubility Parameter δ, and Percentage of *Inter*molecular Hydrogen Bonds for the Microstructures Starting from the Densities of 0.011, 1.0 and 1.5 g/cm³

	density of the initial guess		
	0.011	1.0	1.5
E_{coh}/V	5.2 (±0.5)	7.8 (±0.4)	7.9 (±0.6)
E_{vdW}	2.9	4.2	4.2
E_C	2.3	3.6	3.7
$\Delta E_{el}/V^b$	1.7	1.6	1.2
δ [(J/cm³)$^{1/2}$]	22.8 (±1.1)	27.9 (±0.7)	28.1 (±1.1)
*inter*mol H-bonds (%)	42.5	68.7	71.5

[a] If not stated otherwise, energies are given in units of 10^8 J/m³. [b] $\Delta E_{el} = p^2/(2B)$, where p is pressure and B is bulk modulus, which has been taken from Sala[79] and equals 0.125 GPa^{-1}.

The cohesive energy densities E_{coh}/V and the solubility parameters δ for the three model structures are displayed in Table 3. The model structures with the higher amount of helical conformations showed the lowest cohesive energy density, whereas the model structures started at higher densities reached 50% higher values.

An experimental value for the cohesive energy density of destructurized starch (0.5% of water) has been derived[60] from temperature-dependent measurements of the activity of water in thermoplastic starch using the relation of Guillet[78] and equaled 12.1 × 10^8 J/m³. Note that the high pressure in the modeled structures could influence the cohesive energy density. The elastic energy stored in the model structures was calculated and is shown in Table 3. If this contribution is taken into account, the cohesive energy density of the model structures is increased to 9.4 × 10^8 J/m³ and lays within 25% of the experimental value.

From the results on the cohesive energy density it was concluded that the model structures started at the lowest density do not represent the starch structure correctly. The remaining types of model structures differ by their distribution of glycosidic linkages between regions I and II (see Influence of the Starting Density). Since there aare no experimental data on this subject, a definitive decision for one of the types of model structures could not be made. If not stated otherwise, all further results refer to the model structures started at a density of 1.0 g/cm³.

The cohesive energy density of model structures can be correlated with the number of *inter*molecular hydrogen bonds. Figure 8 shows that there exists a direct proportionality between the cohesive energy density of the single cubes and the number of *inter*molecular hydrogen bonds per repeat unit. This suggests that the cohesive energy density of dry starch may be dependent on the conformation.

Table 3 shows that the Coulombic part, E_C, of the *inter*molecular energy is slightly smaller than the van der Waals, E_{vdW}, energy term. From Figure 9 it can be seen that the *inter*molecular energy is varying strongly from one repeat unit to another. The mean value was 19.3 kcal/mol with an rms deviation of 4.4 kcal/mol. An inspection of the pair distribution functions (Figure 10) showed that the significant *inter*molecular distance correlations can be attributed to hydrogen bonds (see g_{O-O}, g_{O-H} and g_{H-H}). If the entire *inter*molecular energy is attributed to hydrogen-bonding interaction alone, a hydrogen-bond energy of approximately 9.5 kcal/mol results. However, a more accurate calculation would require separately considering the interactions between nonpolar groups and would reduce this value.

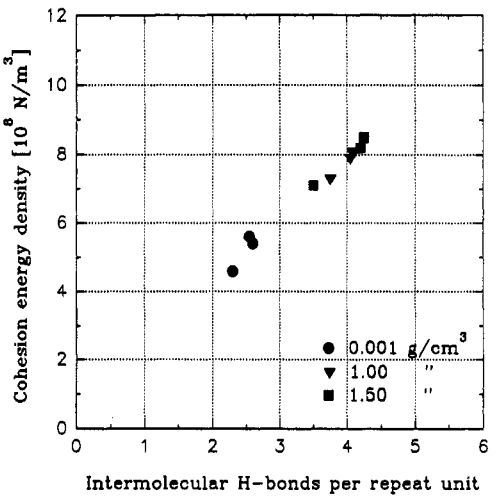

Figure 8. Cohesive energy density E_{coh}/V in 10^8 N/m³ versus the number of *inter*molecular hydrogen bonds per repeat unit for all the simulated microstructures of amorphous starch. The densities of the initial guess structures are 0.001 (circles), 1.0 (triangles), and 1.5 g/cm³ (squares).

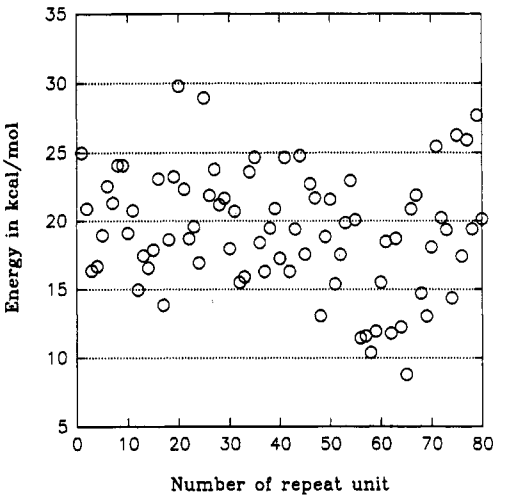

Figure 9. *Inter*molecular energy in kcal/mol per repeat unit in one of the microstructures plotted versus the number of the repeat unit.

Structure and Radial Distribution Function. The *inter*- and *intra*molecular pair distribution functions, $g_{\alpha-\beta}$, were evaluated for all the $\alpha-\beta$ atom pairs in the system. The *intra*molecular pair distribution functions showed characteristic sharp peaks at low distances for the atoms separated by one or a few bonds. They contain mainly structural information on the repeat unit and were not sensitive to a variation of the conformation at the glycosidic linkage (not shown). The *inter*molecular pair distribution functions (Figure 10) showed the characteristic increase to values near 1 at the higher distances. For the oxygen and hydrogen pairs they exhibited sharp correlations at distances corresponding to hydrogen bonds. As described above, the *inter*molecular structure of starch was very much dominated by hydrogen bonding.

Figure 11 shows the differential radial distribution functions $4\pi r^2\Delta\varrho^x$ derived from the model structure and from the X-ray scattering intensity of destructurized starch. (The difference in the $\Delta\varrho^x$'s of the microstructures started at density 1.0 and 1.5 g/cm³ was very small, so that all six microstructures were used for the derivation of $\Delta\varrho^x$). The agreement between experimental and modeled distribution functions (Figure 11) was very good for the positions of the first two peaks. The somewhat lower and broader first peak of the experi-

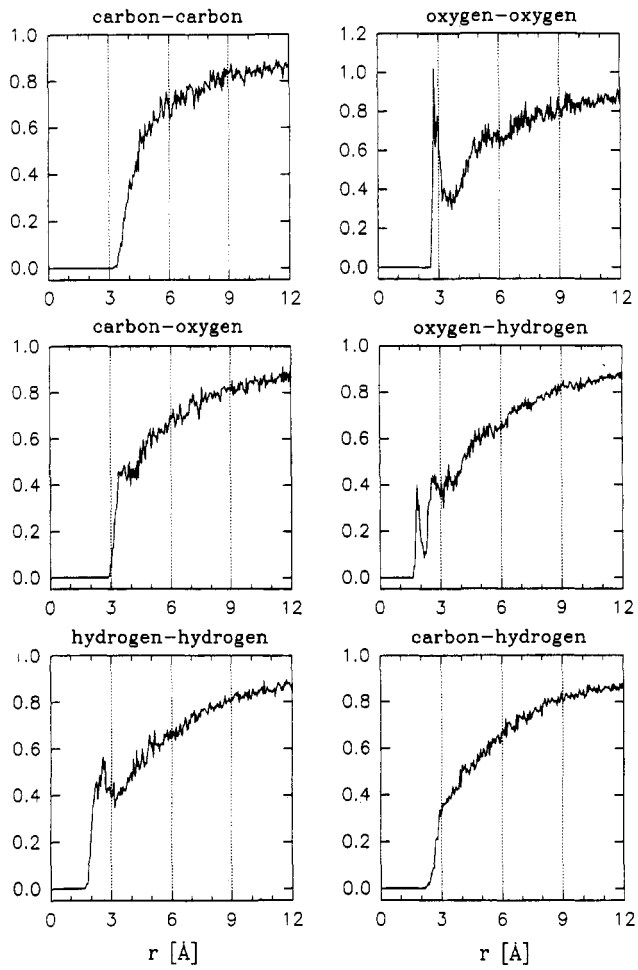

Figure 10. *Inter*molecular pair distribution functions $g_{\alpha-\beta}$ for all the atom pairs in the model structure.

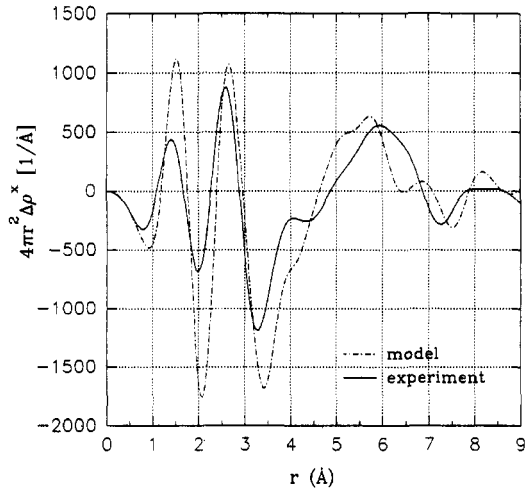

Figure 11. Differential radial distribution function $4\pi r^2\Delta\varrho^x$ derived from model structures (solid) and from the X-ray scattering experiments (dashed).

mental differential radial distribution function could be attributed to the limited experimental scattering angle region.[67] The first two peaks represent the distance between nearest neighbors in the structure, i.e., mainly between chemically bonded atoms. The first peak contains *intra*molecular distances from the different bond lengths in the molecule. The second peak contains *intra*molecular distances from atoms, which are two bonds apart, and an *inter*molecular contribution from the hydrogen-bonded oxygen atoms (see Figure 10).

For the second group of peaks (between 3 and 7 Å), the agreement was less satisfactory. Still, all the peak positions up to a distance of ca. 6 Å, which are found by experiment were also present in the model. In this region of the $4\pi r^2\Delta\varrho^x$ the maxima contain *intra*molecular distances (e.g., the distance between successive glycosidic oxygen atoms of ca. 4.5 Å) as well as *inter*molecular ones. At higher distances than ca. 6 Å, there was no more agreement between experiment and model. In this region the experimental differential radial distribution function is increasingly affected by the quality of the sample surface on one hand. On the other hand, in the modeled distribution function, the low number of microstructures led to an increased noise of the curve, which is greatly enhanced at higher distances.

Conclusions

It has been shown that with the proposed method a structure of amorphous starch can be simulated that shows a differential radial distribution function comparable to the one derived from X-ray scattering experiments for distances up to 6 Å. The model structure allowed a molecular view of the specific interactions of the starch chains, which were shown to be dominated by the interactions of the polar hydroxyl groups. The atom pair distribution functions of the model structure were marked by strong correlations at distances corresponding to hydrogen bonds, and the mean number of hydrogen bonds was 7.8 per repeat unit. The mean number of hydrogen bonds per hydroxyl group was found to be 2.3 (of maximal 3) and the ring and the glycosidic oxygen only contributed to approximately 10% of all hydrogen bonds. 56% of all the hydrogen bonds in the model structure were *inter*molecular. The hydrogen bonds occurred in a wide variety of geometries.

A comparison of model structures with different chain conformations suggested that the high cohesive energy density of amorphous starch is mainly determined by the high density of *inter*molecular hydrogen bonds. Structures with a low portion of *inter*molecular hydrogen bonds seemed less likely to represent the structure of amorphous starch. The cohesive energy density of the model structure was 9.4×10^8 J/m^3, which corroborates the high cohesive energy density found experimentally.

However, two points have to be mentioned. The first is that the used force field is not optimized to fit carbohydrates, which resulted in the very high pressure of the model structures. The influence of this pressure on the derived properties is difficult to estimate and an improvement of the force field parameters would clearly be desirable. The second is that the chain branching, which is an important feature of the amylopectin molecule, has completely been neglected.

The model structure contained a considerable amount of "cellulosic" conformations (high ψ-values). Such conformations have up to now only been experimentally confirmed in the small molecule of maltose.

Nevertheless, these simulations seemed to reveal a fundamentally correct representation of the structure of amorphous starch. They showed that this material is strongly networked by hydrogen bonds, giving rise to its high glass transition temperature. The use of a low molecular weight plasticizer will certainly modify these interactions, and the following contribution[19] investigates the effects of water molecules on the hydrogen-bonding network of the amorphous starch structure.

Acknowledgment. We gratefully acknowledge support by Grant Nos. 20-27840.89 and 20-32209.91 of the Swiss National Fund for Scientific Research. We are also very grateful to Prof. U. W. Suter and his modeling group for many helpful discussions and support.

References and Notes

(1) Whistler, R. L.; BeMiller, J. N.; Paschall, E. F. *Starch Chemistry and Technology*, 2nd ed.; Academic Press: Orlando, 1984.
(2) Tomka, I.; Wittwer, F. Eur. Pat. Appl. 118240, P: 51 pp, CL: C08L3/00, PRTY APPL:467982 (US), YR:1983 (18.02.83) PAT APPL:84/300940, YR:1984 (14.02.84), 1983.
(3) Tomka, I.; Stepto, R. F. T.; Dobler, B. Eur. Pat. Appl. 282451, P: 9 pp, CL:C08B30/12, PRTY APPL:87/5442 (GB), YR:1987 (09.03.87) PAT APPL:88/810130, YR:1988 (02.03.88), 1987.
(4) Tomka, I.; Stepto, R. F. T.; Thoma, M. Eur. Pat. Appl. 304401, P: 14 pp, CL:C08L3/02, PRTY APPL:87/19485 (GB), YR:1987 (18.08.87), PAT APPL:88/810548, YR:1988 (12.08.88), 1987.
(5) Willenbücher, R. W.; Tomka, I.; Müller, R. *Carbohydrates in industrial Synthesis*; Proc. Symp. Div. Carb. Chem. Am. Chem. Soc.; Verlag Dr. A. Bartens: Berlin, 1992; pp 93–111.
(6) Tomka, I. *Water Relationships in Foods*; Levine, H., Slade, L., Eds.; Plenum Press: New York, 1991; pp 627–637.
(7) Zobel, H. F.; Rocca, L. A. *Cereal Chem.* **1988**, *65*, 443–446.
(8) Imberty, A.; Buléon, A.; Tran, V.; Pérez, S. *Starch/Stärke* **1991**, *43*, 375–384.
(9) French, D. *Starch: Chemistry and Technology*, 2nd ed.; Whistler, R. L., BeMiller, J. N., Paschall, E. F., Eds.; Academic Press: Orlando, 1984; pp 184–247.
(10) Imberty, A.; Pérez, S. *Int. J. Biol. Macromol.* **1989**, *11*, 177–185.
(11) Buléon, A.; Tran, V. *Int. J. Biol. Macromol.* **1990**, *12*, 345–352.
(12) Gidley, M. J.; Bociek, S. M. *J. Am. Chem. Soc.* **1985**, *107*, 7040–7044.
(13) Gidley, M. J.; Bociek, S. M. *J. Am. Chem. Soc.* **1988**, *110*, 3820–3829.
(14) Brant, D. A.; Christ, M. D. *Computer Modeling of Carbohydrate Molecules*; French, A. D., Brady, J. W., Eds.; ACS Symposium Series 430; American Chemical Society: Washington, DC, 1990; pp 42–68.
(15) Banks, W.; Greenwood, C. T. *Starch and its Components*; Edinburgh University Press: Edinburgh, 1975.
(16) Pérez, S.; Vergelati, C. *Polym. Bull.* **1987**, *17*, 140–147.
(17) Ring, S. G.; l'Anson, K. J.; Morris, V. J. *Macromolecules* **1985**, *18*, 182–188.
(18) Tomka, I. EP 397819 (3.11.88), 1988.
(19) Trommsdorff, U.; Tomka, I. *Macromolecules*, following paper in this issue.
(20) Theodorou, D. N.; Suter, U. W. *Macromolecules* **1985**, *18*, 1467–1478.
(21) Hutnik, M.; Gentile, F. T.; Ludovice, P. J.; Suter, U. W.; Argon, A. S. *Macromolecules* **1991**, *24*, 5962–5969.
(22) Ludovice, P. J.; Suter, U. W. *Comput. Mod. Polym.* **1992**, 401–435.
(23) Rapold, R. F.; Suter, U. W.; Theodorou, D. N. *Makromol. Theory Simul.* **1994**, *3*, 1–17.
(24) Arizzi, S.; Mott, P. H.; Suter, U. W. *J. Polym. Sci., Part B: Polym. Phys.* **1992**, *30*, 415–426.
(25) Gusev, A. A.; Suter, U. W. *Phys. Rev.* **1991**, *A43*, 6488.
(26) Gusev, A. A.; Suter, U. W. *J. Chem. Phys.* **1993**, *99*, 2228–2234.
(27) Hutnik, M.; Argon, A. S.; Suter, U. W. *Macromolecules* **1991**, *24*, 5970–5973.
(28) Theodorou, D. N.; Suter, U. W. *Macromolecules* **1986**, *19*, 139–154.
(29) Argon, A. S.; Mott, P. H.; Suter, U. W. *Phys. Stat. Solidi B* **1992**, *172*, 193–204.
(30) Hutnik, M.; Argon, A. S.; Suter, U. W. *Macromolecules* **1993**, *26*, 1097–1108.
(31) Gusev, A. A.; Müller-Plathe, F.; van Gunsteren, W. F.; Suter, U. W. *Adv. Polym. Sci.* **1994**, *116*, 207–247.
(32) Gentile, F. T.; Suter, U. W. *Material Science and Technology*; Thomas, E. L., Ed.; VCH Weinheim, 1993; pp 34–77.
(33) Klug, H. P.; Alexander, L. E. *X-Ray Diffraction Procedures*; John Wiley & Sons: New York, 1974.
(34) Maple, J.; Dinur, U.; Hagler, A. T. *Proc. Natl. Acad. Sci. U.S.A.* **1988**, *85*, 5350–5354.
(35) Maple, J. R.; Thacher, T. S.; Dinur, U.; Hagler, A. T. *Chem. Design Autom. News* **1990**, *5*, 5–10.
(36) Weiner, S. J.; Kollmann, P. A.; Case, D. A.; Singh, U. C.; Ghio, C.; Alagona, G.; Profeta, S., Jr.; Weiner, P. *J. Am. Chem. Soc.* **1984**, *106*, 765–784.
(37) Weiner, S. J.; Kollmann, P. A.; Nguyen, D. T.; Case, D. A. *J. Comput. Chem.* **1986**, *7*, 230–252.
(38) Discover 2.9, BIOSYM Technologies, San Diego, 1993.
(39) Maple, J. R.; Hwang, M.-H.; Stockfisch, T. P.; Dinur, U.; Waldmann, M.; Ewig, C. S.; Hagler, A. T. *J. Comput. Chem.* **1994**, *15*, 162–182.
(40) Sun, H.; Mumby, S. J.; Maple, J. R.; Hagler, A. T. *J. Am. Chem. Soc.* **1994**, *116*, 2978–2987.
(41) Sun, H.; Mumby, S. J.; Maple, J. R.; Hagler, A. T. *J. Am. Chem. Soc.*, accepted.
(42) Homans, S. W. *Biochemistry* **1990**, *29*, 9110–9118.
(43) French, A. D.; Rowland, R. S.; Allinger, N. L. *Computer Modeling of Carbohydrate Molecules*; French, A. D., Brady, J. W., Eds.; ACS Symposium Series 430; American Chemical Society: Washington, DC, 1990; pp 120–140.
(44) Arnott, S.; Scott, W. E. *J. Chem. Soc., Perkin Trans. 2* **1972**, 324–335.
(45) Trommsdorff, U. Dissertation 10758, ETH-Zurich, 1994.
(46) Jeffrey, G. A. *Acta Crystallogr.* **1990**, *B46*, 89–103.
(47) Goebel, C. V.; Dimpfl, W. L.; Brant, D. A. *Macromolecules* **1970**, *3*, 644–654.
(48) Tran, V.; Buléon, A.; Imberty, A.; Pérez, S. *Biopolymers* **1989**, *28*, 679–690.
(49) Sundararajan, P. R.; Rao, V. S. R. *Biopolymers* **1969**, *8*, 313–323.
(50) Pérez, S.; Roux, M.; Revol, J. F.; Marchessault, R. H. *J. Mol. Biol.* **1979**, *129*, 113–133.
(51) Pérez, S.; Taravel, F.; Vergelati, C. *Nouv. J. Chim.* **1985**, *9*, 561–564.
(52) Ha, S. N.; Madsen, L. J.; Brady, J. W. *Biopolymers* **1988**, *27*, 1927–1952.
(53) Brady, J. W.; Schmidt, R. K. *J. Phys. Chem.* **1993**, *97*, 958–966.
(54) Dowd, M. K.; Zeng, J.; French, A. D.; Reilly, P. J. *Carbohydr. Res.* **1992**, *230*, 223–244.
(55) Imberty, A.; Pérez, S. *Biopolymers* **1988**, *27*, 1205–1221.
(56) Imberty, A.; Chanzy, H.; Pérez, S.; Buleon, A.; Tran, V. *J. Mol. Biol.* **1988**, *201*, 365–378.
(57) Born, M.; von Karmann, T. *Phys. Z.* **1912**, *13*, 297–309.
(58) Metropolis, N.; Rosenbluth, A. W.; Rosenbluth, M. N.; Teller, A. H.; Teller, E. *J. Chem. Phys.* **1953**, *21*, 1087–1092.
(59) Jordan, R. C.; Brant, D. A.; Cesaro, A. *Biopolymers* **1978**, *17*, 2617–2632.
(60) Benczédi, D., personal communication.
(61) van den Berg, C. B. Dissertation, Wageningen, The Netherlands, 1981.
(62) Berendsen, H. J. C.; Postma, J. P. M.; van Gunsteren, W. F.; DiNola, A.; Haak, J. R. *J. Chem. Phys.* **1984**, *81*, 3684–3690.
(63) Verlet, L. *Phys. Rev.* **1967**, *159*, 98–103.
(64) Cotton, J. P.; Decker, D.; Benoit, H.; Farnoux, B.; Higgins, J.; Jannik, G.; Ober, R.; Picot, C.; des Cloiseaux, J. *Macromolecules* **1974**, *7*, 863–872.
(65) Debye, P. *Ann. Phys.* **1915**, *46*, 809.
(66) Warren, B. E. *X-Ray Diffraction*; Addison-Wesley Publishing Company: Reading, MA, 1969; pp 116–149.
(67) Alexander, L. E. *X-Ray Diffraction Methods in Polymer Science*; R. E. Krieger Publishing Company: Huntington, NY, 1985.
(68) Schubach, H. R. Dissertation, Ulm, 1984.
(69) *International Tables of X-Ray Crystallography*; The Kynoch Press: Birmingham, 1974; Vol. IV.
(70) Smith, V. H., Jr.; Thakkar, A. J.; Chapman, D. C. *Acta Crystallogr.* **1975**, *A31*, 391–392.
(71) Weick, D. *Ann. Phys.* **1970**, *7*, 143–167.
(72) Krogh-Moe, J. *Acta Crystallogr.* **1956**, *9*, 951–953.
(73) Yanez, M.; Steward, R. F. *Acta Crystallogr.* **1978**, *A34*, 648–651.
(74) Lorch, E. *J. Phys. C, Ser. 2* **1969**, *2*, 229–237.
(75) Jeffrey, G. A.; Rosenstein, R. D. *Adv. Carbohydr. Chem.* **1964**, *19*, 7–22.
(76) Savage, H. F. J.; Finney, J. L. *Nature* **1986**, *322*, 717–720.
(77) Allen, M. P.; Tildesley, D. J. *Computer Simulations of Liquids*; Clarendon Press: Oxford, 1992.
(78) DiPaola, G.; Guillet, J. E. *Macromolecules* **1978**, *11*, 228–235.
(79) Sala, R.; I. Tomka, I. *The Glassy State in Foods*; Blanshard, J. M. V., Lillford, P. J., Eds.; Nottingham University Press: Nottingham, 1993; pp 475–489.

MA946348U